https://doi.org/10.5194/egusphere-2026-2058
Preprint. Discussion started: 12 May 2026
© Author(s) 2026. CC BY 4.0 License.

Influence of synoptic patterns (NAO vs. WeMO) on rainfall isotopic composition in SE Iberia: A machine learning approach

Artur Stachnik[1,2], Fernando Gázquez[3,4], Antonio Lope Morales-González[5], Mario Morellón[1], Antonio González-Ramón[6], Francisco Moral-Martos[7], Rosario Jiménez-Espinosa[5] and Javier Martín-Chivelet[1,2]

[1]Department of Geodynamics, Stratigraphy, and Paleontology, Complutense University of Madrid, Madrid, 28040, Spain.
[2]Geoscience Institute (IGEO), CSIC-UCM, Madrid, 28040, Spain.
[3]Department of Biology and Geology, University of Almeria, Almeria, 04120, Spain.
[4]Andalusian Center for Global Change-Hermelindo Castro, University of Almeria, Almeria, 04120, Spain.
[5]Department of Geology of the University of Jaén, Jaén, 23071, Spain.
[6]Geological and Mining Institute of Spain (IGME-CSIC), Madrid, 28003, Spain.
[7]Department of Physical, Chemical and Natural Systems, Pablo de Olavide University, Seville, 41013, Spain.

Correspondence to: Artur Stachnik (artursta@ucm.es)

Abstract. Atmospheric circulation controls moisture transport across the western Mediterranean, but its seasonally resolved imprint on precipitation isotopes in many areas remains poorly understood, limiting the integration of circulation diagnostics with modern isotope monitoring. Southeastern Iberia constitutes an outstanding natural laboratory to identify and quantify the roles and isotopic footprint of the main modes of atmospheric variability in the region (i.e., the Western Mediterranean Oscillation (WeMO) and the North Atlantic Oscillation (NAO)) and other local factors, such as altitude and precipitation amount. Here, we combine a multi-altitude (560–1800 m a.s.l.) precipitation-isotope network in Sierra de Segura, a mountain range located in SE Spain with explainable machine-learning methods to quantify how large-scale circulation and precipitation regime control rainfall isotopic composition.

First we extend the WeMO index forward from 2020, when instrumental measurements end, to 2025 using a physically constrained XGBoost reconstruction based on regional sea-level pressure predictors from San Fernando (Spain) and multiple northern Italian stations, reproducing the published index over 2010–2020 with robust cross-validated performance ($R^2 = 0.85 \pm 0.05$; RMSE = 0.41 ± 0.07, $n = 129$ months). Then we analyze 448 rainwater samples collected between 2017 and 2023, aggregated into 154 precipitation-weighted monthly observations of $\delta^{18}O$, $\delta^{2}H$ and $\delta^{17}O$, together with d-excess and ^{17}O-excess. Bulk isotope ratios co-vary strongly ($\rho > 0.95$), allowing $\delta^{18}O$ to represent the dominant network-scale signal.

Random Forest models interpreted using SHAP reveal a clear seasonal reorganization of controls. During the wet season (October–March), $\delta^{18}O$ variability is primarily circulation-driven, with the North Atlantic Oscillation acting as the dominant control and the WeMO providing a consistent secondary modulation. In contrast, during the dry season (April–September), $\delta^{18}O$ is governed by precipitation regime, with precipitation amount overwhelmingly predominating over circulation indices and exhibiting a strongly non-linear, amount-effect response. Back-trajectory clustering of regionally coherent isotope-sampling events supports these contrasting seasonal influences, indicating a small number of recurrent synoptic transport regimes in winter and weaker synoptic organization in summer.

Overall, these results provide a transferable, seasonally calibration that links synoptic circulation and precipitation regime to rainfall $\delta^{18}O$ (and excess parameters) in southeastern Iberia. This innovative framework enables robust interpretation of Mediterranean isotope-based paleoclimate archives by distinguishing circulation-driven wet-season signals from precipitation-regime-driven dry-season variability. It is readily applicable to other climatically complex areas influenced by multiple modes of atmospheric variability and pronounced seasonal contrasts. Furthermore, our results provide a basis for assessing the sensitivity of cave and lake systems to future changes in circulation persistence and rainfall intermittency under ongoing climate change.

1 Introduction

The climate of the Iberian Peninsula is strongly shaped by synoptic-scale atmospheric variability, as a result of its particular location at the southwestern margin of Europe, where mid-latitude and subtropical circulation regimes interact. This setting produces pronounced seasonal and interannual hydroclimatic variability and high sensitivity to shifts in large-scale atmospheric circulation (Quesada et al., 2012; Pereira et al., 2021). Such variability not only governs modern precipitation dynamics, but also conditions how atmospheric signals are integrated and preserved in continental geological archives across Iberia. Therefore, understanding these seasonal dynamics is crucial for a correct understanding and interpretation of palaeohydrological records in the region.

At synoptic scale, Iberian hydroclimate is primarily organized by North Atlantic pressure fields, among which the subtropical anticyclone (Azores High) plays a central role. Seasonal changes in its intensity and position modulate the balance between summer subsidence and cold-season westerly advection. During autumn and winter, enhanced Atlantic zonal flow and extratropical cyclone activity constitute the main mechanisms for moisture transport into Iberia and are closely linked to the North Atlantic Oscillation (NAO), the dominant mode of Euro-Atlantic variability (Hurrell et al., 1995). Positive NAO phases are typically associated with drier Iberian winters due to northward storm-track displacement, whereas negative phases favor wetter conditions, particularly in western and southern regions. Consistent with this, NAO variability is negatively correlated with winter precipitation, river discharge and water resources across the Iberian Peninsula (Trigo et al., 2004). According to palaeohydrological reconstructions, this correlation has also been operating during the last millennia and it has been responsible for the occurrence of the main wet and dry periods, such as the Medieval Climate Anomaly and the Little Ice Age (Moreno et al., 2012; Morellón et al., 2012; Hernández et al., 2020). In particular, southern Iberian lake records have revealed that summer atmospheric relative humidity during Roman times was also influenced by NAO (Gázquez et al., 2025). Because these circulation anomalies primarily act by reorganizing moisture transport and precipitation pathways, stable water isotopes in precipitation provide a direct, physically grounded tracer of circulation-driven hydroclimatic variability, and constitute a key link between atmospheric dynamics and isotopic signals preserved in speleothems and lacustrine systems.

Beyond North Atlantic forcing, regional pressure gradients within the western Mediterranean also modulate Iberian hydroclimate. This variability has been described through the Western Mediterranean Oscillation (WeMO), a regional pressure pattern reflecting differences between the southwestern Iberian Peninsula and the central Mediterranean basin (Martín-Vide et al., 2008; López-Bustins et al., 2020). The WeMO provides a coherent diagnostic of the western Mediterranean pressure dipole and has become widely used in Iberian hydroclimate studies. Positive WeMO phases are generally associated with reduced precipitation over Iberia, whereas negative phases favor moist southerly to southwesterly advection and wetter conditions (Martín-Vide & López-Bustins, 2006; López-Bustins et al., 2008). Although NAO and WeMO operate at different spatial scales and may interact, their combined influence and relative seasonal roles over southeastern Iberia remain debated.

Despite its widespread use, a practical limitation currently restricts WeMO-based analyses of modern observational datasets: published WeMO index values are not available after 2020. Because the original WeMOi formulation relies on specific reference stations (San Fernando in Spain, and Padua in Italy), continuity depends on the availability and publication of those series. The lack of updated values beyond 2020 therefore represents an instrumental discontinuity rather than a conceptual limitation, yet it directly hampers the interpretation of recent monitoring records and the calibration of circulation–isotope relationships relevant for Holocene proxy records. In the context of the ongoing climate change, improving our understanding of how synoptic-scale patterns interact is increasingly important, as projected trends toward more persistent positive NAO conditions are expected to intensify drought in the western Mediterranean (Smith et al., 2025).

Resolving these circulation influences requires observational frameworks capable of linking synoptic variability with physically interpretable hydroclimatic tracers. Stable oxygen and hydrogen isotopes are a fundamental tool for investigating the hydrological cycle and atmospheric moisture transport, owing to their sensitivity to phase-change processes and to key physical variables such as temperature and humidity (Clark and Fritz, 1997). Precipitation-isotope monitoring in Iberia remains spatially sparse, with long-term continuity largely provided by the Spanish Network of Isotopes in Precipitation (REVIP) and the Global Network of Isotopes in Precipitation (GNIP) (Díaz-Teijeiro et al., 2005). While peninsula-scale syntheses capture first-order spatial patterns in $\delta^{18}O$–$\delta^{2}H$ and deuterium excess, seasonal process attribution remains limited by heterogeneous sampling strategies and incomplete overlap with circulation diagnostics (Hatvani et al., 2020). Recent studies have begun to bridge this gap by explicitly linking rainfall isotopes to meteorological conditions, air-mass pathways, and kinetic effects using bulk and triple-oxygen isotope observations (Moreno et al., 2021; Giménez et al., 2021).

Southeastern Iberia represents an ideal natural laboratory, located at the intersection of dominant Atlantic and Mediterranean moisture sources and influenced by the interaction between NAO and WeMO. Yet the seasonal imprint of these circulation modes on the isotopic composition of precipitation in this region has not been systematically quantified. Such analyses are essential for interpreting isotope-based paleoclimate archives across the western Mediterranean, including speleothems (Cisneros et al., 2021) and lake sediments (Toney et al., 2020; Gázquez et al., 2025), particularly where recharge seasonality and circulation persistence exert competing controls.

Here we investigate the controls on precipitation isotopy in southeastern Iberia using a multi-altitude monitoring network Sierra de Segura (~38°17′N, ~2°40′W; 560–1800 m a.s.l.). Because the published WeMO index is available only until December 2020 while isotope monitoring extends into subsequent years (2021–2024), establishing a temporally consistent circulation predictor is a prerequisite for isotope–climate attribution. Thus, we extend the published WeMOi beyond 2020 using a physically constrained, data-driven framework calibrated against the existing record. Our objective is not to redefine or improve upon the original formulation, but to preserve strict compatibility with the published index while enabling its application to recent observational datasets. We subsequently combine this extended index with the NAO, precipitation amount, and topographic controls to quantify the seasonal hierarchy of drivers governing precipitation isotopy. By integrating correlation analysis, dimensionality reduction, and explainable modelling, this framework provides a seasonally explicit separation between circulation-driven and precipitation-regime-driven isotope signals and clarifies their implications for modern observations and the interpretation of isotope-based paleoclimate archives in the western Mediterranean region.

2 Methods

2.1 Reconstruction of the Western Mediterranean Oscillation Index

2.1.1 Data compilation and preprocessing

Four northern Italian stations (Malo, Venezia, Teolo, Cavallino) were selected to represent the central–northern Italian pressure field associated with the eastern pole of the WeMO dipole. These stations are located within the Veneto region and the adjacent Po Plain sector, geographically close to Padua, the original eastern reference station of the WeMO formulation, and embedded within the same synoptic-scale pressure regime. Using multiple stations rather than relying on a single substitute for Padua reduces sensitivity to potential station-specific inhomogeneities and captures the shared regional pressure signal that underlies the original Padua–San Fernando configuration (Martín-Vide & López-Bustins, 2006; López-Bustins et al., 2008). This regional representation preserves the large-scale dynamical structure of the index while maintaining fidelity to its original dipole concept.

The available Western Mediterranean Oscillation index (WeMOi) was obtained from the original publication (Martín-Vide & López-Bustins, 2006). The WeMOi column was programmatically identified, converted to numeric format, and paired with parsed Year–Month components extracted from the original Date field. All SLP datasets and observed WeMOi values were subsequently merged into a unified monthly modelling table spanning 2010–2025.

© Author(s) 2026. CC BY 4.0 License.

2.1.2 WeMOi predictor construction

Given that the Western Mediterranean Oscillation (WeMO) index represents a large-scale pressure dipole between the Gulf of Cádiz and northern Italy, physically meaningful predictors were derived using two complementary strategies.
First, sea-level pressure (SLP) values were extracted for each station to retain the full synoptic signal. Second, spatial pressure gradients were computed to explicitly represent the dipolar pressure contrast underlying the WeMO structure. Specifically, pressure differences between San Fernando and each of the four northern Italian stations were calculated as:

$$D_{Station} = SLP_{San\ Fernando} - SLP_{Station}$$

Seasonality was incorporated using a cyclic transformation of the month variable to avoid artificial discontinuities between December and January. Each month "m" was mapped to a phase angle.

$$\theta = 2\pi \frac{m-1}{12}$$

and encoded as:

$$month\_\sin = \sin(\theta), \qquad month\_\cos = \cos(\theta)$$

The final predictor set therefore consisted of 11 variables: five SLP values, four inter-station pressure gradients, and two cyclic seasonal terms. The target variable was the observed WeMO index (WeMOobs). Only months between 2010 and 2020 with complete SLP coverage and non-missing WeMOobs were retained for model training (n = 129).

2.1.3 Machine Learning framework

A gradient-boosted regression tree model implemented in XGBoost (Chen and Guestrin, 2016) was employed to capture potential non-linear relationships and higher-order interactions among predictors. The model was trained using a squared-error objective function. Hyperparameter tuning was performed using a randomized search strategy combined with cross-validation, in which sixty candidate hyperparameter combinations were sampled from predefined parameter distributions (Table 1). For each configuration, a 5-fold K-fold cross-validation procedure (with shuffle enabled and a fixed random state) was applied, and model selection was based on the minimization of cross-validated mean squared error (MSE). After identifying the optimal hyperparameter set, model performance was assessed using an independent 10-fold cross-validation procedure to obtain robust estimates of predictive skill (R^2, RMSE and MAE). Finally, the model was refitted using the full 2010–2020 dataset to obtain the final trained estimator.

Parameter	Distribution / values tested
n_estimators	200, 400, 600, 800, 1000
max_depth	2, 3, 4, 5
learning_rate	0.01, 0.02, 0.03, 0.05, 0.07, 0.1
subsample	0.7, 0.8, 0.9, 1.0
colsample_bytree	0.6, 0.7, 0.8, 0.9, 1.0
min_child_weight	1, 3, 5, 7
gamma	0.0, 0.1, 0.2
reg_lambda	0.5, 1.0, 1.5, 2.0

Table 1: Hyperparameter search space explored during randomized cross-validated model optimization.

2.1.4 Reconstruction of the synthetic WeMO index

The final model, WeMO_PhysicallyConstrained_Multistation_XGB, obtained after cross-validated hyperparameter optimization and refitted on the complete 2010–2020 training dataset, was applied to generate WeMOi predictions for the period January 2021 to December 2025. Model predictions were computed only for months with complete predictor availability.

A continuous monthly timeline spanning January 1950 to December 2025 was constructed. The final synthetic WeMO index (WeMOi) was assembled by retaining observed WeMOi values for the period 1950–2020 and using model-derived estimates for the period 2021–2025. The resulting dataset was exported as a monthly time series (Date, WeMOi).

2.2 Precipitation Isotopy & Climate Relationships for the Sierra de Segura

2.2.1 Isotopic Data Acquisition

During the period from December 2017 to March 2023, eight rain collectors were installed at different elevations (Table 2; Fig. 1) across the study area. Each sampling unit consisted of a plastic bottle equipped with a funnel and containing approximately 20 ml of paraffin oil to prevent evaporation. The bottles were retrieved and replaced with new ones during each survey, and the collected water was quantified and subsampled for isotope analysis in the laboratory. This rainwater sampling method has been shown to be more reliable than conventional rain collectors (i.e., tube-dip-in-water collectors) for stable isotope studies in low-rainfall regions (Natali et al., 2022). Sampling was conducted approximately every 1-2 months. In total, 448 rainwater samples were collected.

Type	Name	Nº samples	Sampling period	X	Y	Altitude (m a.s.l.)
Rain	RC1	43	25/12/2017–26/03/2023	529930	4234070	1800
Rain	RC2	48	03/05/2020–26/03/2023	529820	4235380	1600
Rain	RC3	53	15/05/2020–26/03/2023	530330	4233200	1400
Rain	RC4	96	25/12/2017–26/03/2023	536120	4240440	1274
Rain	RC5	57	25/12/2017–26/03/2023	530160	4238770	1024
Rain	RC6	53	25/12/2017–18/12/2022	529520	4240310	780
Rain	RC7	46	01/01/2018–18/12/2022	525750	4242930	603
Rain	RC8	52	25/12/2017–26/03/2023	522190	4245630	562

Table 2: Summary of precipitation sampling sites (RC1–RC8) in the Sierra de Segura monitoring network, including number of collected samples, sampling period, and site coordinates. X and Y correspond to UTM easting and northing in ETRS89 / UTM zone 30N, and Z indicates altitude (meters above sea level).

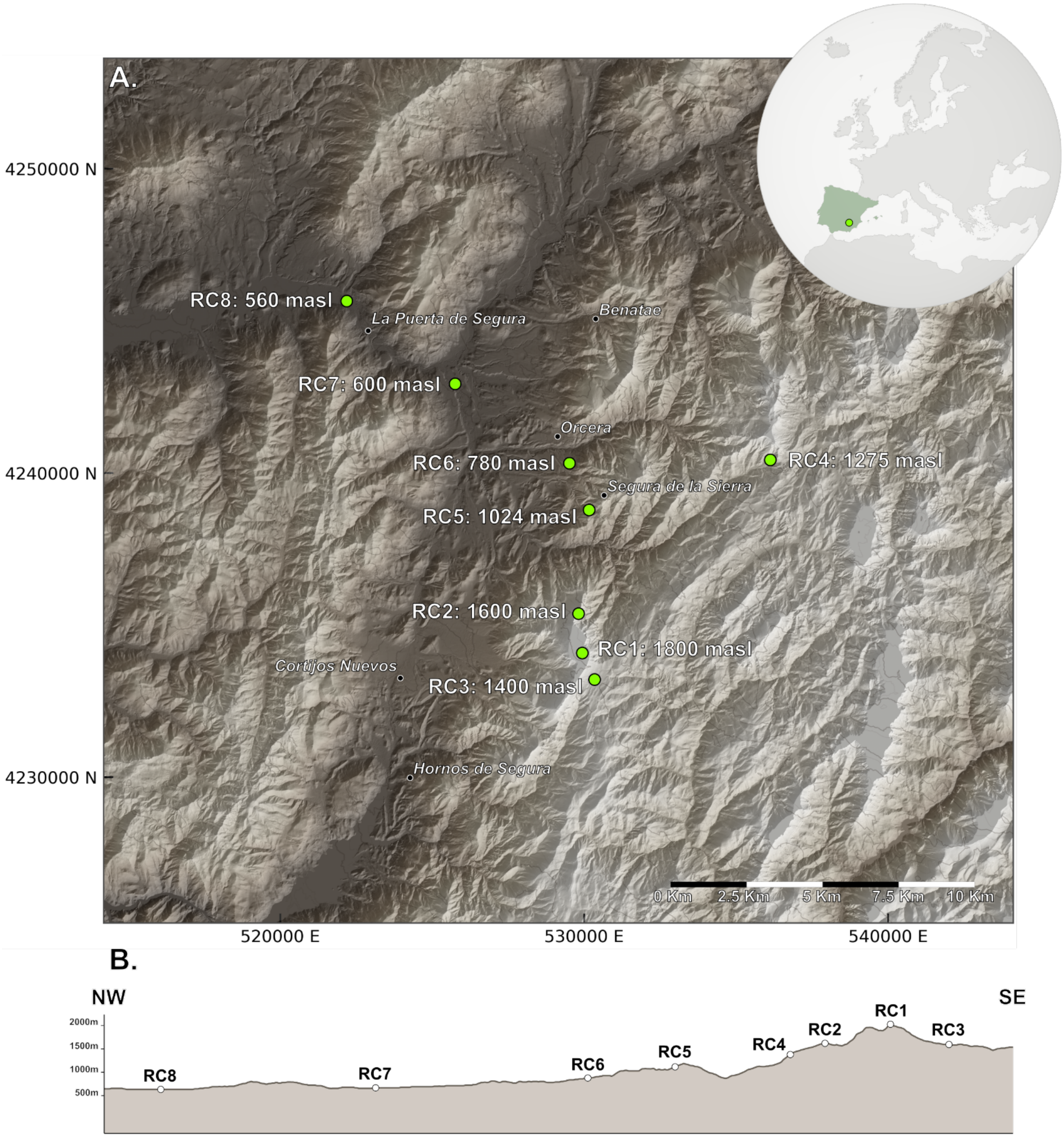

Figure 1. (A) Map of the eight rain-collector sites (RC1–RC8) in the Sierra de Segura, distributed along an altitudinal transect from 560 to 1800 m a.s.l. Topography is shown as shaded relief, and the inset indicates the location of the study area within the Iberian Peninsula. (B) Idealized topographic profile of the transect (NW–SE) showing the relative elevation and position of the rain-collector sites.

The oxygen and hydrogen isotopic compositions of rainwater were measured using cavity ring-down spectroscopy (CRDS; Steig et al., 2014) with a Picarro L2140-i analyzer at the Laboratory of Stable Isotopes, University of Almería, Spain. The results were normalized to the V-SMOW scale by analyzing internal standards before and after each batch of 12–15 samples. Three internal water standards were calibrated against Vienna Standard Mean Ocean Water (V-SMOW2), Standard Light Antarctic Precipitation (SLAP2), and Greenland Ice Sheet Precipitation (GISP) reference materials. All isotopic deviations are reported in per mil (‰) relative to V-SMOW. Long-term analytical precision (1σ) was assessed by repeated measurements of an internal standard every 5–6 samples and was ±0.1‰ for δ^{18}O and ±0.6‰ for δ^{2}H (n = 90). The ^{17}O-

https://doi.org/10.5194/egusphere-2026-2058
Preprint. Discussion started: 12 May 2026
© Author(s) 2026. CC BY 4.0 License.

excess results were calibrated using the approach of Schoenemann et al. (2013). This standardization considers ^{17}O-excess=0 for V-SMOW and SLAP. The mean ^{17}O-excess precision was 14 per meg, based on the 7 consecutive injections of each sample.

2.2.2 Monthly Aggregation of Event-Based Isotopic Data

Event-based precipitation samples collected at the monitoring stations listed in Table 2 were aggregated to monthly resolution using precipitation-weighted averaging following the standard methodology adopted by the Global Network of Isotopes in Precipitation (GNIP, IAEA). Secondary isotopic parameters (d-excess and ^{17}O-excess) were subsequently calculated using conventional formulations. All monthly variables (δ^{18}O, δ^{17}O, δ^{2}H, d-excess, ^{17}O-excess, and precipitation totals) were screened for missing values, internal consistency, and physically implausible outliers prior to subsequent analyses. The resulting monthly dataset spans 2017–2023, with temporal coverage determined by the availability of field-collected precipitation events. Monthly large-scale circulation indices were appended to the isotopic dataset to enable climate–isotope analyses. The NAO index (NAOi) was obtained from the NOAA Climate Prediction Center. The WeMO index (WeMOi) was obtained from the CRU repository for 1950–2020 and extended for 2021–2025 using the *WeMO_PhysicallyConstrained_Multistation_XGB* model described in Sect. 2.1. All atmospheric indices were parsed to monthly resolution and temporally aligned with the isotopic dataset prior to statistical analyses (See Sect. S1 for full mathematical formulations).

2.2.3 Seasonal Partitioning of Hydroclimatic Regimes

Precipitation isotopic data were partitioned into two hydroclimatic seasons commonly used for southeastern Iberia (De Luis et al., 2011): a wet season spanning October–March (ONDJFM) and a dry season spanning April–September (AMJJAS). Seasonal grouping was performed at monthly resolution, based on the precipitation-weighted monthly isotopic dataset described in Sect. 2.2.2. All statistical analyses were conducted separately for wet and dry seasons in order to account for the marked intra-annual hydroclimatic contrast characteristic of the region. Months lacking isotopic determinations were excluded from seasonal analyses.

2.2.4 Statistical framework for isotopy–climate relationships

All statistical analyses were performed on the monthly precipitation-weighted isotopic variables and associated predictors after pre-processing. Wet and dry season subsets were analyzed independently following the seasonal partitioning described above. Pairwise associations among isotopic variables (δ^{18}O, δ^{2}H, δ^{17}O, ^{17}O-excess and d-excess), precipitation amount, station metadata (latitude, longitude, altitude), and atmospheric indices (NAOi and WeMOi) were quantified using Spearman rank correlation coefficients. Correlation matrices were computed separately for wet and dry seasons using available paired observations for each variable combination. Heatmaps were generated to facilitate comparison of correlation structures across seasons. Joint variability among atmospheric predictors, precipitation amount, and station elevation was explored using principal component analysis (PCA), applied independently to wet and dry season subsets. Prior to PCA, variables were standardized using z-score normalization. The analysis yielded explained variance ratios, component loadings, and principal component scores for each season. Results were summarized through scree plots and two-dimensional projections of principal component space. Spatial consistency across the monitoring network was examined by computing station-wise Spearman correlations between isotopic variables (δ^{18}O, ^{17}O-excess and d-excess) and atmospheric predictors (NAOi, WeMOi, and precipitation amount). Correlations were calculated separately for wet and dry seasons using station-level subsets of paired observations. Stations were ordered by altitude for visualization purposes, and relationships were displayed using altitude–correlation scatterplots with a constant horizontal reference line.

2.2.5 Back-trajectory analysis and transport regime classification

To characterize the dominant air-mass transport pathways associated with precipitation recorded on isotope sampling dates, backward trajectory analyses were performed using the Hybrid Single-Particle Lagrangian Integrated Trajectory (HYSPLIT) model (Stein et al., 2015). The analysis was restricted to regionally coherent precipitation events to provide a circulation-scale framework consistent with the spatially integrated isotopic signal and to avoid pseudo-replication of individual synoptic systems across stations. Only dates with available isotope observations were considered.

Daily precipitation at each station was converted to a binary rain/no-rain flag using a threshold of pcp > 0.1 mm. A regional "day with rainfall" was retained when precipitation was recorded at a minimum of four out of eight stations (≥50% of the network), while days failing this criterion were excluded from further analysis. Days with rainfall were subsequently grouped into wet (ONDJFM) and dry (AMJJAS) seasons to maintain consistency with the seasonal framework applied in the isotopic analyses.

Backward air-mass trajectories were computed for each regional day with rainfall using HYSPLIT, initialized at 12:00 UTC and integrated backward for 96 h. A single arrival location was used for all simulations, defined as the geographic centroid of the monitoring network. Trajectories were launched from three arrival heights above ground level (500, 1500, and 3000 m) to sample distinct layers of the lower troposphere and lower free troposphere. Meteorological forcing was provided by the GDAS1 reanalysis. Trajectories were generated independently for each day with rainfall, season, and arrival altitude.

For quantitative comparison of transport pathways, trajectories were represented in a limited trajectory space defined by longitude–latitude coordinates sampled at fixed temporal lags (0, 24, 48, 72, and 96 h prior to arrival). This representation emphasizes large-scale transport geometry while minimizing sensitivity to small-scale curvature near the receptor. Trajectories were clustered separately for each season and arrival altitude using k-means clustering applied to the reduced trajectory vectors, following widely adopted objective transport classification approaches (Dorling et al., 1992). Clustering was initialized with a season-dependent number of clusters, and a post-processing step was applied to merge clusters containing fewer than a minimum number of trajectories in order to avoid poorly populated regimes. As a result, the final number of transport regimes may differ from the initial clustering configuration and reflects the set of statistically robust clusters retained for analysis. For each retained cluster, a representative centroid trajectory was calculated as the mean longitude and latitude at each sampled lag.

To relate transport regimes to large-scale atmospheric circulation, each day with rainfall was associated with monthly values of the North Atlantic Oscillation and Western Mediterranean Oscillation indices corresponding to the month of arrival. For each season–altitude subset, NAOi and WeMOi values were classified into terciles (low, neutral, high) based exclusively on the empirical distribution of index values associated with the reduced set of days with rainfall. The relative contribution of each transport regime within NAOi and WeMOi terciles was subsequently quantified for each season and arrival altitude.

2.2.6 Random Forest modelling and SHAP analysis of isotopy and excess predictors

To investigate how large-scale circulation indices, precipitation amount, and topographic factors jointly structure isotopic variability across the monitoring network, an explainable machine-learning framework based on random forest regression was implemented (Geurts et al., 2006). The framework was applied to monthly $\delta^{18}O$, d-excess, and ^{17}O-excess, and models were fitted independently for wet (ONDJFM) and dry (AMJJAS) season subsets.

For each isotopic target and season, models were trained using four predictors: NAOi, WeMOi, monthly precipitation amount (pcp_sum), and station altitude. Only observations with non-missing values for the target and all predictors were retained for each seasonal model. Predictors were not standardized prior to modelling, consistent with the scale-invariant nature of tree-based methods. Random forest hyperparameters were fixed across all experiments (n_estimators = 300, max_depth = 6, min_samples_split = 3, min_samples_leaf = 2, max_features = √p).

© Author(s) 2026. CC BY 4.0 License.

Model performance and sampling variability were assessed using Monte Carlo cross-validation based on repeated ShuffleSplit partitions. For each season and isotopic target, 200 random splits were generated with 80% of the data used for training and 20% for testing. A random forest regressor was fitted to each training subset and evaluated on the corresponding held-out subset using R^2, mean absolute error (MAE), and root-mean-square error (RMSE). Mean and standard deviation of these metrics across all iterations were used to summarize performance stability.

Final seasonal models were then trained on all available observations for each isotopic target. Predictor relevance was quantified using impurity-based feature importance derived from the fitted random forest, together with permutation importance computed as the reduction in model R^2 following random permutation of each predictor (100 repetitions). To obtain model-agnostic and interpretable estimates of predictor influence, SHAP values were calculated for each final seasonal model using a tree-based SHAP explainer. Global importance was defined as the mean absolute SHAP value per predictor. SHAP dependence plots were generated for selected predictors (NAOi in the wet season and precipitation amount in the dry season) to visualize how variations in each predictor contribute to the isotopic response across its observed range.

3 Results

3.1 Machine-Learning Reconstruction of WeMOi

Cross-validated evaluation of the *WeMO_PhysicallyConstrained_Multistation_XGB* model over the 2010–2020 calibration interval yields a mean coefficient of determination of $R^2 = 0.85 \pm 0.05$ and a mean root-mean-square error of RMSE = 0.41 ± 0.07 WeMOi units (n = 129 months). The model reproduces the principal temporal variability of the published WeMOi series across the overlap period, capturing both positive and negative phases of the oscillation (Fig. 2A). The synthetic WeMOi series constructed in this study combines the official index (1950–2020) with a machine-learning extension for 2021–2025 derived from the calibrated model. The resulting hybrid record (1950–2025) provides a temporally continuous WeMOi series consistent with the statistical structure of the observational index (Fig. 2B).

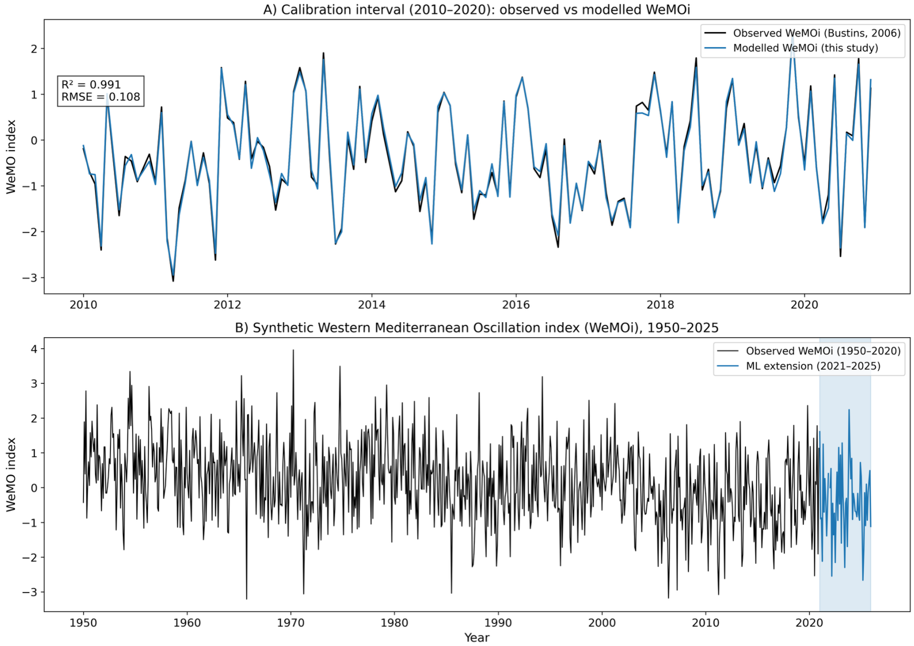

Figure 2A: Calibration interval (2010–2020), showing the official WeMOi series and predictions from the WeMO_PhysicallyConstrained_Multistation_XGB model. Cross-validated performance over the calibration period is

R^2 = 0.85 ± 0.05 and RMSE = 0.41 ± 0.07 (n = 129 months). 2B: Synthetic WeMOi series (1950–2025) constructed in this study by combining the published WeMOi record (1950–2020) with the machine-learning extension for 2021–2025. The shaded region highlights the reconstructed interval.

3.2 Isotopic–Climate Relationships in the Sierra de Segura

3.2.1 Temporal coverage and distribution of isotopic observations

Monthly precipitation-weighted isotopic compositions (δ^{18}O, δ^{2}H, δ^{17}O, d-excess and ^{17}O-excess) were available for eight monitoring sites in the Sierra de Segura between December 2017 and March 2023. The dataset comprises 205 valid monthly observations across the network. Observational coverage varies among stations according to sampling continuity and operational periods. Calendar months were assigned to wet (ONDJFM) and dry (AMJJAS) seasons, yielding 153 wet-season and 52 dry-season observations. This uneven seasonal distribution reflects the predominance of precipitation events during the hydrologically active winter months in southeastern Iberia. This observational structure defines the seasonal and spatial framework within which isotopic–climate relationships are evaluated in the following sections.

3.2.2 Seasonal correlation structure between stable isotopes and atmospheric drivers

Seasonal Spearman correlation matrices (Fig. 3) reveal a consistent internal structure among isotopic variables. The three primary isotope ratios (δ^{18}O, δ^{2}H and δ^{17}O) are strongly and positively correlated in both wet and dry seasons (ρ = 0.96–1.00). In contrast, ^{17}O-excess and d-excess are negatively correlated with the primary isotope ratios, with moderate magnitudes during the wet season (e.g., δ^{18}O–^{17}O-excess: $\rho = -0.31$) and stronger negative correlations during the dry season (δ^{18}O–^{17}O-excess: $\rho = -0.85$; δ^{18}O–d-excess: $\rho = -0.79$). Precipitation amount shows weak correlations with isotopic composition during the wet season (δ^{18}O–pcp_sum: $\rho = -0.01$) and stronger negative correlations during the dry season (δ^{18}O–pcp_sum: $\rho = -0.74$). Atmospheric indices display season-dependent associations. NAOi is negatively correlated with δ^{18}O during the wet season ($\rho = -0.41$) and weakly positively correlated during the dry season ($\rho = +0.08$). WeMOi exhibits a weak positive correlation with δ^{18}O in the wet season ($\rho = +0.23$) and a weak negative correlation in the dry season ($\rho = -0.13$).

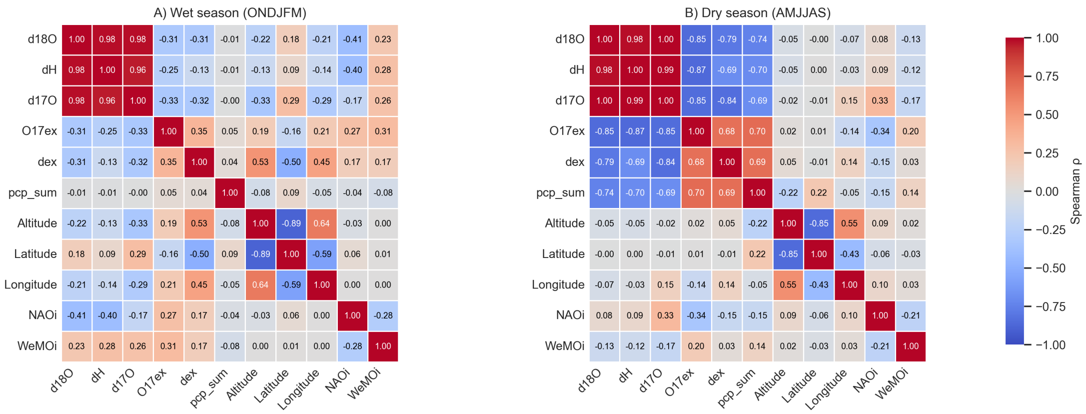

A) Wet season (ONDJFM)

	d18O	dH	d17O	O17ex	dex	pcp_sum	Altitude	Latitude	Longitude	NAOi	WeMOi
d18O	1.00	0.98	0.98	-0.31	-0.31	-0.01	-0.22	0.18	-0.21	-0.41	0.23
dH	0.98	1.00	0.96	-0.25	-0.13	-0.01	-0.13	0.09	-0.14	-0.40	0.28
d17O	0.98	0.96	1.00	-0.33	-0.32	-0.00	-0.33	0.29	-0.29	-0.17	0.26
O17ex	-0.31	-0.25	-0.33	1.00	0.35	0.05	0.19	-0.16	0.21	0.27	0.31
dex	-0.31	-0.13	-0.32	0.35	1.00	0.04	0.53	-0.50	0.45	0.17	0.17
pcp_sum	-0.01	-0.01	-0.00	0.05	0.04	1.00	-0.08	0.09	-0.05	-0.04	-0.08
Altitude	-0.22	-0.13	-0.33	0.19	0.53	-0.08	1.00	-0.89	0.64	-0.03	0.00
Latitude	0.18	0.09	0.29	-0.16	-0.50	0.09	-0.89	1.00	-0.59	0.06	0.01
Longitude	-0.21	-0.14	-0.29	0.21	0.45	-0.05	0.64	-0.59	1.00	0.00	0.00
NAOi	-0.41	-0.40	-0.17	0.27	0.17	-0.04	-0.03	0.06	0.00	1.00	-0.28
WeMOi	0.23	0.28	0.26	0.31	0.17	-0.08	0.00	0.01	0.00	-0.28	1.00

B) Dry season (AMJJAS)

	d18O	dH	d17O	O17ex	dex	pcp_sum	Altitude	Latitude	Longitude	NAOi	WeMOi
d18O	1.00	0.98	1.00	-0.85	-0.79	-0.74	-0.05	-0.00	-0.07	0.08	-0.13
dH	0.98	1.00	0.99	-0.87	-0.69	-0.70	-0.05	0.00	-0.03	0.09	-0.12
d17O	1.00	0.99	1.00	-0.85	-0.84	-0.69	-0.02	-0.01	0.15	0.33	-0.17
O17ex	-0.85	-0.87	-0.85	1.00	0.68	0.70	0.02	0.01	-0.14	-0.34	0.20
dex	-0.79	-0.69	-0.84	0.68	1.00	0.69	0.05	-0.01	0.14	-0.15	0.03
pcp_sum	-0.74	-0.70	-0.69	0.70	0.69	1.00	-0.22	0.22	-0.05	-0.15	0.14
Altitude	-0.05	-0.05	-0.02	0.02	0.05	-0.22	1.00	-0.85	0.55	0.09	0.02
Latitude	-0.00	0.00	-0.01	0.01	-0.01	0.22	-0.85	1.00	-0.43	-0.06	-0.03
Longitude	-0.07	-0.03	0.15	-0.14	0.14	-0.05	0.55	-0.43	1.00	0.10	0.03
NAOi	0.08	0.09	0.33	-0.34	-0.15	-0.15	0.09	-0.06	0.10	1.00	-0.21
WeMOi	-0.13	-0.12	-0.17	0.20	0.03	0.14	0.02	-0.03	0.03	-0.21	1.00

Figure 3: Spearman rank correlation matrices for wet-season months (ONDJFM; A) and dry-season months (AMJJAS); B) across all stations. Variables include isotopic parameters (δ^{18}O, δ^{2}H, δ^{17}O, ^{17}O-excess, d-excess), monthly precipitation amount (pcp_sum), station metadata (altitude, latitude, longitude), and circulation indices (NAOi, WeMOi). Cell values indicate correlation coefficients (ρ), with a common color scale from −1 to +1.

© Author(s) 2026. CC BY 4.0 License.

3.2.3 Principal Component Structure of Atmospheric Predictors

A principal component analysis (PCA) was performed separately for the wet and dry seasons using four predictors: NAOi, WeMOi, monthly precipitation (pcp_sum), and station altitude (Fig. 4). In the wet season, PC1 explains 32.2% of the total 335 variance, followed by PC2 (27.5%) and PC3 (23.8%). In the dry season, PC1 accounts for 30.0% of variance, PC2 for 26.2%, and PC3 for 25.3%.

During the wet season, NAOi and WeMOi display loadings of opposite sign along PC1, while precipitation projects primarily onto PC2. Altitude loads most strongly on PC3, with limited contribution to PC1.

In the dry season, the loading structure differs. NAOi and precipitation both contribute to PC1, while WeMOi exhibits its 340 strongest loading on PC3. Altitude shows substantial projection onto PC1 and PC3. The PC1–PC2 representation therefore indicates a redistribution of variance among predictors relative to the wet season. The full loading matrices for wet and dry seasons are reported in Table S1.

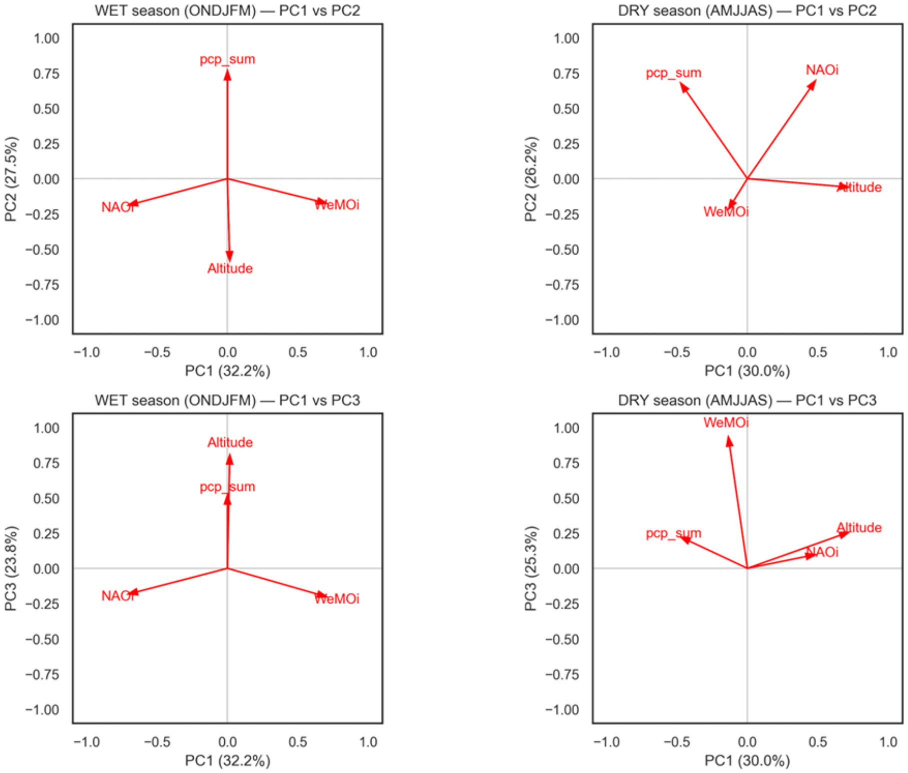

345 **Figure 4: Seasonal principal component analysis (PCA) of atmospheric predictors. Biplots show the orientation and relative magnitude of predictor loadings (NAOi, WeMOi, monthly precipitation, and altitude) for the wet season (ONDJFM; left panels) and dry season (AMJJAS; right panels). Upper panels display PC1–PC2, and lower panels PC1–PC3 projections. Axis labels indicate the percentage of variance explained by each principal component.**

© Author(s) 2026. CC BY 4.0 License.

3.2.4 Station-wise seasonal correlations between isotopy and atmospheric predictors

Spearman correlations between δ¹⁸O and the three predictors (NAOi, WeMOi, and precipitation amount) reveal coherent seasonal structures across the 560–1800 m altitudinal transect (Fig. 5).

During the wet season (ONDJFM), δ¹⁸O shows consistently negative correlations with NAOi across all stations ($\rho = -0.50$ to -0.18) and positive correlations with WeMOi ($\rho = 0.11$ to 0.49). Correlations with precipitation remain weak and close to zero ($\rho = -0.25$ to 0.11), without a systematic elevation-dependent trend.

During the dry season (AMJJAS), the correlation structure differs markedly. At higher-elevation stations (RC1–RC3 and RC5), δ¹⁸O correlates positively with NAOi ($\rho = 0.25$ to 0.70), whereas lower-elevation stations (RC6–RC8) display negative NAOi–δ¹⁸O correlations (down to $\rho = -0.80$). Correlations with WeMOi range from −0.50 to 0.03. In contrast, precipitation exhibits strong negative correlations with δ¹⁸O at most stations ($\rho = -0.86$ to -1.00), with weaker or neutral values at the lowest sites (RC7–RC8).

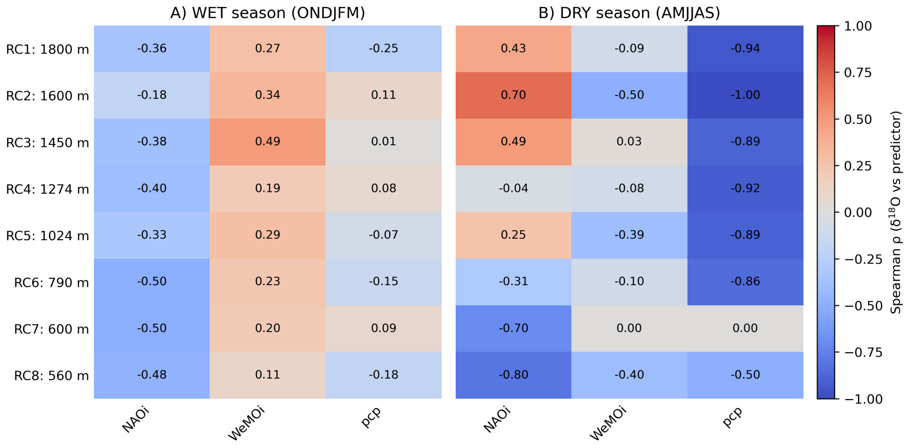

Station	A) NAOi	A) WeMOi	A) pcp	B) NAOi	B) WeMOi	B) pcp
RC1: 1800 m	-0.36	0.27	-0.25	0.43	-0.09	-0.94
RC2: 1600 m	-0.18	0.34	0.11	0.70	-0.50	-1.00
RC3: 1450 m	-0.38	0.49	0.01	0.49	0.03	-0.89
RC4: 1274 m	-0.40	0.19	0.08	-0.04	-0.08	-0.92
RC5: 1024 m	-0.33	0.29	-0.07	0.25	-0.39	-0.89
RC6: 790 m	-0.50	0.23	-0.15	-0.31	-0.10	-0.86
RC7: 600 m	-0.50	0.20	0.09	-0.70	0.00	0.00
RC8: 560 m	-0.48	0.11	-0.18	-0.80	-0.40	-0.50

Figure 5: Station-wise Spearman correlations between monthly isotopic variables and atmospheric predictors. Heatmaps show Spearman correlation coefficients (ρ) between δ¹⁸O and NAOi, WeMOi, and precipitation amount for the wet season (ONDJFM; A) and dry season (AMJJAS; B). Stations are ordered by altitude (highest at top). A common color scale ($\rho = -1$ to 1) is used across panels.

Station-wise correlations computed for ¹⁷O-excess and d-excess against the same predictors (Figs. S1–S2) display greater spatial heterogeneity. During the wet season, both excess metrics exhibit mixed positive and negative correlations across stations and predictors. In the dry season, ¹⁷O-excess shows predominantly positive correlations with precipitation ($\rho = 0.77$ to 1.00 where defined), while NAOi correlations are generally negative at higher elevations. For d-excess, dry-season correlations with precipitation are predominantly positive ($\rho = 0.48$ to 0.90), whereas associations with NAOi and WeMOi vary in sign across stations.

3.2.5 Atmospheric transport regimes associated with isotopic precipitation events

A total of 52 regionally coherent days with rainfall coincident with isotope sampling were identified (Table S2), comprising 40 wet-season (ONDJFM) and 12 dry-season (AMJJAS) events. For each day with rainfall, backward air-mass trajectories were computed at three arrival heights (500, 1500, and 3000 m above ground level), yielding 156 trajectories for quantitative analysis.

https://doi.org/10.5194/egusphere-2026-2058
Preprint. Discussion started: 12 May 2026
© Author(s) 2026. CC BY 4.0 License.

Clustering of backward trajectories reveals a limited number of statistically robust transport regimes, with the final number varying by season and arrival height (Table S3). During the wet season, three regimes are retained at 500 and 1500 m, and four regimes at 3000 m. During the dry season, two regimes are retained at 500 and 3000 m, whereas the 1500 m subset collapses to a single regime. Silhouette values range from 0.227 to 0.393 for wet-season subsets and from 0.325 to 0.410 for dry-season subsets where more than one regime is retained (Table S3).

To illustrate the transport structure in the main text, we present the wet-season subset arriving at 1500 m (n = 40; K_final = 3; silhouette = 0.393) and the dry-season subset arriving at 500 m (n = 12; K_final = 2) (Fig. 6). Cluster-mean trajectories summarize the dominant large-scale transport pathways for each subset, with individual trajectories grouped around each mean pathway. An overview of centroid trajectories for all season–altitude combinations is provided in Fig. S3. The relative contribution of transport regimes across terciles of NAOi and WeMOi, computed exclusively from the same set of days with rainfall, is shown in Fig. 6 for the subsets highlighted in the main text. The complete set of tercile-stratified regime distributions for all season–altitude combinations is provided in Fig. S4. Differences in regime frequency across circulation terciles are evident in both seasons, although interpretation of the dry-season subsets remains constrained by the smaller number of events (n = 12). Full clustering diagnostics (initial and final K, silhouette values, and cluster sizes) are summarized in Table S3.

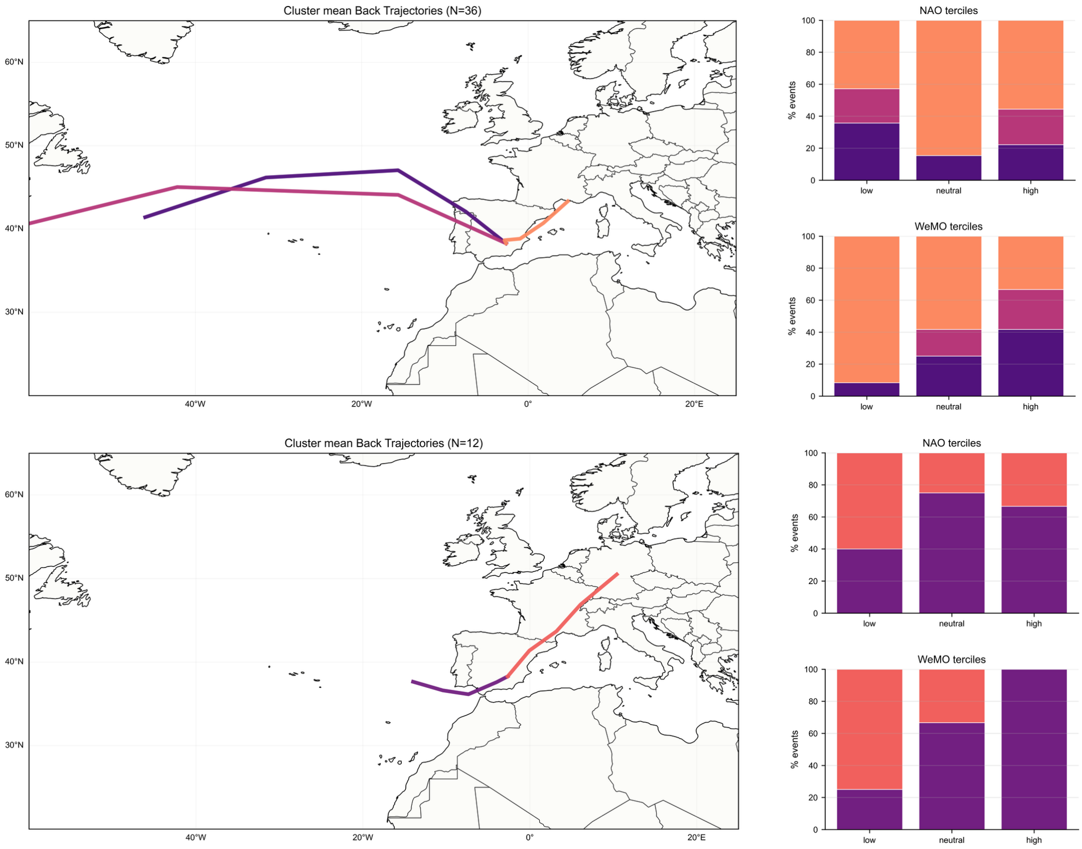

Figure 6: Atmospheric transport regimes associated with precipitation events. Cluster-mean backward trajectories for A: wet-season events arriving at 1500 m (n = 40; K_final = 3; silhouette = 0.393) and B: dry-season events arriving at 500 m (n = 12; K_final = 2). Bold lines represent cluster means. Bar charts show the relative frequency of regimes

across terciles of NAOi and WeMOi computed from the same set of “days with rainfall”. Percentages are normalized within each tercile.

3.2.6 Machine-learning and explainable-AI characterization of isotopic controls

To quantify the relative contribution of atmospheric circulation, precipitation amount, and topographic factors to monthly δ^{18}O variability, Random Forest models were trained separately for the wet and dry seasons. Model performance was evaluated using Monte Carlo cross-validation (200 shuffle–split iterations; 80/20 partitioning) and summarized through R², RMSE and MAE statistics (Table S4). During the wet season (ONDJFM), the model achieved $R^2 = 0.48 \pm 0.14$ and RMSE = 1.43 ± 0.23‰ (n = 145). Permutation importance indicated that NAOi exerted the strongest control on model skill, followed by WeMOi, precipitation amount and altitude (Fig. S5). SHAP global importance values reproduced this hierarchy (Fig. 7A), with NAOi contributing the largest mean absolute effect on predicted δ^{18}O. The SHAP dependence plot highlights the continuous modelled response of δ^{18}O across the observed NAOi range (Fig. 7B).

In contrast, during the dry season (AMJJAS), model performance increased to $R^2 = 0.60 \pm 0.25$ and RMSE = 1.46 ± 0.40‰ (n = 52). Here, precipitation amount emerged as the dominant predictor according to permutation importance (Fig. S5), with NAOi exerting a secondary influence. SHAP global importance values mirrored this redistribution of predictor influence (Fig. 7C), showing precipitation as the primary contributor to predicted δ^{18}O variability, followed by NAOi. The SHAP dependence plot illustrates the modelled δ^{18}O response across the precipitation domain (Fig. 7D).

The same seasonal Random Forest and explainable-AI workflow was applied to d-excess and ^{17}O-excess (Figs. S6–S9; Table S4). Model skill is lower and more variable for these metrics, particularly for ^{17}O-excess in the wet season (n = 88) and dry season (n = 37). For d-excess, R² values are 0.43 ± 0.14 (wet, n = 145) and 0.35 ± 0.36 (dry, n = 52). For ^{17}O-excess, R² values are 0.20 ± 0.23 (wet, n = 88) and 0.40 ± 0.40 (dry, n = 37). Despite reduced skill relative to δ^{18}O, the seasonal reordering of predictor influence remains evident: altitude ranks highest for d-excess in the wet season, whereas precipitation amount dominates in the dry season; for ^{17}O-excess, WeMOi ranks highest in the wet season, while precipitation amount is the dominant contributor in the dry season.

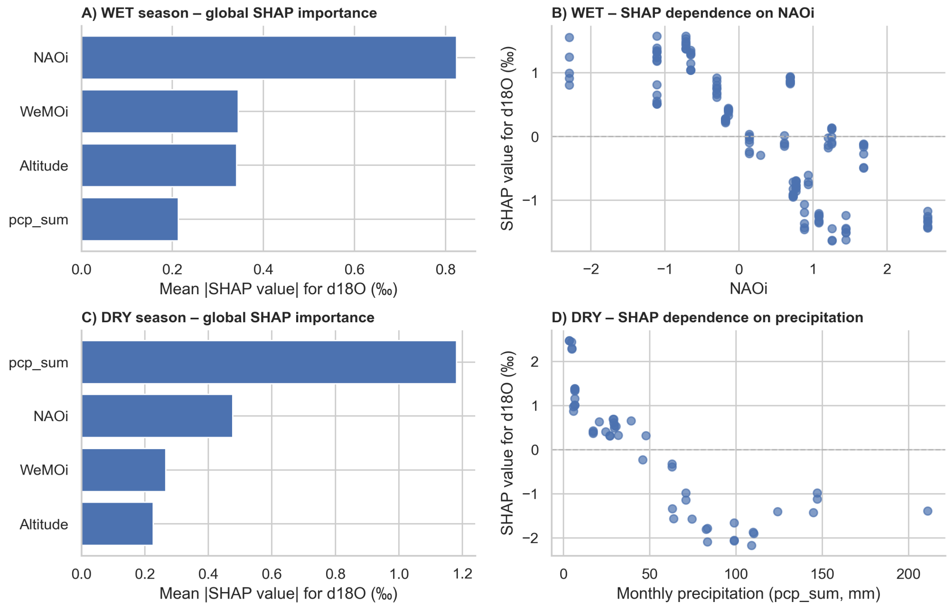

https://doi.org/10.5194/egusphere-2026-2058
Preprint. Discussion started: 12 May 2026
© Author(s) 2026. CC BY 4.0 License.

Figure 7: SHAP-based importance and dependence plots for the seasonal Random Forest $\delta^{18}O$ models. A: Global SHAP importance for the wet season (ONDJFM). B: SHAP dependence of $\delta^{18}O$ on NAOi in the wet season. C: Global SHAP importance for the dry season (AMJJAS). D: SHAP dependence of $\delta^{18}O$ on monthly precipitation amount in the dry season. Positive SHAP values indicate positive contributions to predicted $\delta^{18}O$.

4 Discussion

4.1 Machine-learning extension of the WeMOi

The machine-learning extension of the WeMOi presented here addresses a practical limitation in the application of this index arising from the absence of continuous, homogenized monthly sea-level pressure data from Padua after 2020, which prevents a direct extension of the index following its original formulation (Martín-Vide & López-Bustins, 2006; López-Bustins et al., 2008). This discontinuity hampered our study, focused on recent hydroclimatic variability and modern monitoring datasets, where circulation indices must temporally overlap with instrumental or geochemical observations.

Using an XGBoost framework trained over the 2010–2020 overlap period, with San Fernando and multiple northern Italian pressure stations as predictors, we demonstrate that the WeMOi can be reproduced with high fidelity at monthly resolution (Fig. 2). The close agreement between observed and modelled values during cross-validation cross-validated performance ($R^2 = 0.85 \pm 0.05$; RMSE = 0.41 ± 0.07) and calibration ($R^2 = 0.99$; RMSE = 0.11) indicates that the regional pressure configuration underlying the original Padua–San Fernando dipole is effectively preserved when Padua is represented by a multi-station northern Italian proxy. Importantly, the reconstructed series reproduces both the sign and amplitude of month-to-month variability, which constitute the primary characteristics exploited in climatological and hydroclimatic applications of the index (Serrano-Notivoli et al., 2018; López-Bustins & Lemus-Canovas, 2020).

Model calibration is constrained by the availability of harmonized monthly pressure records from the Italian station network, accessible only from 2010 onwards. The 2010–2020 interval therefore represents the maximum period over which the published WeMOi and complete predictor data coexist. Within this limitation, the hybrid series retains the officially published index unchanged from 1950 to 2020 and applies the machine-learning reconstruction exclusively beyond the observational endpoint. In doing so, the historical structure, amplitude, and sign characteristics of the WeMOi are preserved, ensuring full compatibility with previous WeMO-based climatological studies (Fig. 2).

The framework adopted here exploits the shared regional pressure signal captured by multiple northern Italian stations, consistent with previous evidence that the WeMOi reflects a regional-scale pressure configuration rather than the characteristics of any single station (López-Bustins et al., 2008; González-Hidalgo et al., 2011). Representing the eastern pole through a regional pressure field rather than a single observational point enhances operational resilience to potential data gaps, while remaining faithful to the conceptual structure of the original WeMO formulation. As long as a coherent regional pressure signal is available, future discontinuities in individual stations would not automatically interrupt the continuity of the index.

From a methodological perspective, this approach provides a reproducible and extensible pathway for maintaining the WeMOi over time without reprocessing the full historical datasets used in its original derivation. Although the present study extends the index to 2025, the same framework can be applied prospectively as new pressure observations become available. Because the extension is calibrated against the official series and preserves its statistical structure, future operational implementations could enable automated, near-real-time propagation of the index without redefining its historical baseline. Such developments would facilitate continued application of the WeMOi in hydroclimatic monitoring, isotope-based research, and broader western Mediterranean climate analyses.

4.2 Seasonal atmospheric controls on a SE Iberian precipitation isotope network

Precipitation-isotope observations within Iberia have provided reasonably robust large scale spatial patterns, yet seasonal process attribution has remained limited by sparse coverage and heterogeneous sampling strategies (Díaz-Teijeiro et al. 2005; Hatvani et al. 2020). Recent process-oriented studies demonstrate that bulk isotope ratios can track circulation and air-mass pathways, whereas excess parameters encode additional source–boundary-layer and post-condensation effects that are harder to capture with monthly indices alone (Moreno et al. 2021; Giménez et al. 2021). Against this backdrop, our SE Iberian station network provides a unified, station-resolved seasonal comparison that quantifies a wet-season circulation-dominated mode and a dry-season precipitation-regime-dominated mode, while also testing how consistently these controls project across stations.

Across the network, the three primary isotope parameters (δ^{18}O, δ^{17}O, and δ^{2}H) share closely aligned covariance structures in both seasons, indicating a strong common mode of variability at network scale (Fig. 3). Within this system, δ^{18}O captures the structure of the bulk isotopic signal and shows the most stable, interpretable links to atmospheric predictors at monthly resolution, supporting its use as the primary tracer for mesoscale analyses of circulation and seasonal precipitation regimes (Bowen & Wilkinson, 2002; Bowen, 2010).

By contrast, ^{17}O-excess and d-excess are less uniformly organized by circulation indices and precipitation totals than δ^{18}O, and they show greater station-to-station variability. Rather than being a limitation, this behaviour is informative: excess parameters provide complementary sensitivity to processes that are largely invisible to bulk isotope ratios, including kinetic fractionation and source–boundary-layer influences such as evaporation, sub-cloud exchange, and near-source humidity/temperature effects (Luz & Barkan, 2010; Pfahl & Sodemann, 2014; Uechi & Uemura, 2019). Consistent with this, our analyses indicate that seasonal structure is still detectable, particularly a stronger link to precipitation variability in the dry season, while circulation-related influences appear more context-dependent. In this way, the excess metrics help constrain the interpretation of δ^{18}O by highlighting when mesoscale and microphysical controls likely modulate the monthly signal beyond what is captured by large-scale indices alone. This added process sensitivity is consistent with the broader station-to-station dispersion observed for the excess metrics in our correlation matrices and explainable-RF diagnostics (Figs. S6–S9), particularly in the dry season when sub-cloud exchange is expected to be more active under low humidity (Giménez et al. 2021).

4.2.1 Wet Season: Circulation-Driven δ^{18}O Variability

During the wet season, δ^{18}O exhibits coherent, station-consistent relationships with large-scale circulation, with the NAO emerging as the dominant control and the WeMO acting as a secondary, modulating mode. The sign structure of the station-wise correlations indicates that NAO-related variability is expressed broadly across the network, while WeMO contributes an additional systematic component that co-varies with the large-scale circulation state. In contrast, correlations with monthly precipitation amount (pcp_sum) are comparatively weaker, consistent with wet-season δ^{18}O being organized primarily by synoptic moisture delivery and upstream rainout history rather than by month-to-month fluctuations in local totals under predominantly stratiform precipitation conditions (Rozanski et al., 1993; Pfahl & Sodemann, 2014).

PCA clarifies this hierarchy by separating circulation and precipitation into distinct predictor dimensions (Fig. 4). In the wet season, PC1–PC2 are dominated by the circulation indices (NAOi and WeMOi, with opposing signs), whereas precipitation amount projects largely orthogonally, reinforcing that circulation variability and precipitation totals represent different modes at monthly scale. Importantly, PC3 captures a largely altitudinal dimension: station altitude loads primarily on PC3, indicating that elevation exerts a measurable control on the isotopic system but does not define the leading circulation-driven structure (Rozanski et al., 1993; Pfahl & Sodemann, 2014). This structure is mirrored in the station-by-station correlations (Fig. 5, Figs. S1–S2), where higher-altitude sites tend to display slightly stronger and more internally consistent δ^{18}O–circulation relationships, plausibly reflecting enhanced coupling to free-tropospheric flow and reduced sensitivity to local

https://doi.org/10.5194/egusphere-2026-2058
Preprint. Discussion started: 12 May 2026
© Author(s) 2026. CC BY 4.0 License.

boundary-layer recycling relative to low-elevation stations, as pointed by Rozanski et al. (1993), Bowen (2010), and Pfahl & Sodemann (2014).

Event-day transport diagnostics provide a mechanistic complement to these monthly patterns. Backward trajectories computed with HYSPLIT and grouped using objective clustering concepts (Dorling et al., 1992) show that wet-season isotope-sampling days with rainfall are delivered by a small number of recurrent synoptic pathways. For the most representative wet-season subset (arrival at 1500 m) (Fig. 6), two dominant regimes are consistent with coherent Atlantic transport geometries, whereas a third regime reflects a more Mediterranean–Iberian pathway. The tercile analysis indicates that the Mediterranean regime is preferentially expressed under neutral NAO conditions and negative WeMO terciles, whereas alternative circulation states favor the Atlantic-dominated regimes (Fig. S4). This association is physically coherent with the role of NAO–WeMO pressure configurations in shaping the balance between Atlantic westerly advection and Mediterranean–Iberian moisture delivery, and supports that wet-season δ^{18}O–circulation signal partly reflects changes in the frequency of distinct transport pathways and their associated condensation/rainout histories, as pointed by Rozanski et al. (1993) and Pfahl & Sodemann (2014). This also suggests that similar circulation-driven variability may be expressed across the wider SE Iberian sector under comparable synoptic regimes.

4.2.2 Dry Season: Precipitation-Driven δ^{18}O Variability

During the dry season, δ^{18}O shifts toward precipitation-regime dominance. At monthly resolution, δ^{18}O becomes more tightly linked to precipitation amount, consistent with amount-effect behaviour under convective precipitation and strong event intermittency. In this regime, transitions between isolated low-amount months, and months with more intense rainfall can exert disproportionate influence on precipitation-weighted δ^{18}O through changes in storm efficiency, sub-cloud exchange, and within-storm rainout structure (Dansgaard, 1964; Gat, 1996; Pfahl & Sodemann, 2014). Correspondingly, the circulation signal weakens: WeMO-related coherence is reduced, and NAO-related relationships tend to diminish and can invert sign relative to the wet season, indicating that dry-season δ^{18}O is less directly organized by a single synoptic circulation mode.

PCA captures this seasonal reorganization by shifting precipitation amount into the leading component. In the dry season, precipitation amount dominates PC1, while NAOi, WeMOi and altitude redistribute onto secondary axes, demonstrating that the leading mode of monthly variability is precipitation-driven rather than circulation-driven. Altitude becomes less prominent as a coherent organizing axis, consistent with convective organization and event-scale heterogeneity obscuring systematic thermal gradients in monthly aggregates (Dansgaard, 1964; Gat, 1996; Pfahl & Sodemann, 2014). During the dry season, the clearest coherent feature for the excess metrics is the precipitation-related signal, consistent with stronger roles for convective organization and sub-cloud exchange under low humidity (Figs. S6–S9).

Trajectory diagnostics also reflect this limited synoptic coherence. Relative to the wet season, the dry-season “day with rainfall” set yields fewer distinguishable regimes and a less stable clustering outcome, consistent with both a smaller number of events that are coherent across the network and a stronger role for mesoscale/convective organization. At 1500 m, the limited number of dry-season events constrain robust identification of a clear recurrent transport regime. At lower altitude (500 m), two broad modes are apparent, one more Atlantic and another more Mediterranean–Iberian, yet their tercile stratification should be interpreted cautiously given sampling limitations. Within these constraints and given the limited number of dry-season events (n = 12), Mediterranean–Iberian transport appears more frequently under negative WeMO and negative NAO terciles, whereas neutral-to-positive NAO/WeMO conditions favour the Atlantic mode. This qualitative pattern is consistent with the observed seasonal weakening/inversion of circulation correlations and underscores that, in the dry season, δ^{18}O variability is governed primarily by precipitation-regime structure (amount-effect behaviour) rather than by a stable synoptic transport geometry (Dansgaard, 1964; Gat, 1996; Pfahl & Sodemann, 2014).

4.2.3 Quantifying the hierarchy of precipitation isotopy controls: Random Forest and SHAP

Overall, these wet–dry contrasts suggest a clear seasonal re-ordering of controls, motivating a quantitative ranking of predictor importance using an explainable machine-learning framework (Random Forests interpreted with SHAP). This approach provides an explicit within-season hierarchy of predictors and resolves the response shape through which dominant drivers contribute to δ^{18}O, enabling a direct comparison between the wet and dry regimes.

In the wet season, SHAP importance is dominated by NAOi, with WeMOi emerging as a consistent secondary contributor, whereas precipitation amount and altitude contribute comparatively little. The SHAP dependence on NAOi is approximately linear across the sampled range, with more positive NAO associated with lower δ^{18}O and negative NAO with higher δ^{18}O, quantifying a wet-season circulation-controlled isotope mode consistent with synoptic reorganization of transport and rainout history over the North Atlantic–western Mediterranean sector (Hurrell et al., 1995; Trigo et al., 2002; Rozanski et al., 1993; Pfahl & Sodemann, 2014). The smaller but systematic role of WeMOi is compatible with additional modulation of western Mediterranean pressure gradients and pathway geometry, refining the wet-season baseline without displacing the NAO as the dominant axis of variability (Martín-Vide & López-Bustins, 2006; Pfahl & Sodemann, 2014). The key wet-season result is therefore not only the dominance of circulation predictors, but also the fact that their influence is expressed through a simple, nearly linear sensitivity over the observed range.

In the dry season, the SHAP hierarchy reorganizes sharply, with precipitation amount (pcp_sum) overwhelmingly dominating model sensitivity while circulation indices contributing weakly. The SHAP dependence on precipitation is strongly non-linear, characterized by increasing δ^{18}O values under low precipitation, a rapid depletion as monthly rainfall increases, and values near to saturation at higher amounts. This response shape quantitatively captures an amount-effect behaviour expected under warm-season convective regimes in this setting, where shifts from intermittent/weak events to more intense rainfall disproportionately alter precipitation-weighted isotopic composition through changes in condensation efficiency, within-storm structure and sub-cloud processes (Dansgaard 1964; Gat 1996; Risi et al. 2008; Pfahl & Sodemann 2014; Giménez et al. 2021). Thus, SHAP provides the quantitative capstone to the preceding seasonal interpretation by explicitly ranking controls and revealing the contrasting response shapes that distinguish the circulation-dominated wet-season mode from the amount-dominated dry-season mode.

Applying the same Monte-Carlo RF–SHAP framework to the excess metrics confirms the seasonal re-ordering of controls but also highlights their greater process complexity (Figs. S6–S9). For ^{17}O-excess, wet-season predictability is low (Monte-Carlo $R^2 \approx 0.20$), consistent with a stronger imprint of moisture-source and boundary-layer relative humidity and associated kinetic effects that are only partially represented by monthly NAO/WeMO and precipitation totals (Luz and Barkan 2010; Giménez et al. 2021). Among the available predictors, WeMOi and altitude provide the strongest contributions in the wet season, whereas in the dry season the limited sample size and higher uncertainty reduce predictive robustness; nevertheless, both the correlation matrices and the explainable-RF diagnostics suggest a more coherent precipitation-related signal under dry-season conditions, consistent with enhanced roles for convective intermittency and sub-cloud exchange (Pfahl & Sodemann 2014; Giménez et al. 2021). For d-excess, altitude ranks highest in the wet season, while precipitation amount dominates in the dry season, and the remaining predictors show weaker and more variable contributions. This behaviour aligns with the view that d-excess integrates multiple interacting processes (source conditions, mixing, and post-condensation kinetic exchange), limiting its interpretation as a single-process tracer in atmospheric diagnostics (Natali et al. 2022).

4.3 Implications for present and past climate variability in the western Mediterranean

By combining multivariate statistics with explainable machine-learning, our Sierra de Segura station network provides a process-based calibration linking circulation and precipitation regime to precipitation δ^{18}O and to the isotopic composition of meteoric recharge recorded by continental archives (Clark and Fritz 1997; Leng and Marshall 2004; McDermott 2004;

https://doi.org/10.5194/egusphere-2026-2058
Preprint. Discussion started: 12 May 2026
© Author(s) 2026. CC BY 4.0 License.

Fairchild and Baker 2012). Although local, the dominant drivers (NAO, WeMO and precipitation amount) operate at synoptic to regional scales, making the inferred wet–dry hierarchy a transferable, testable framework for comparable western Mediterranean areas.

During the wet season, isotopic variability is governed primarily by large-scale atmospheric circulation, with a near-linear dependence on the North Atlantic Oscillation and a secondary but coherent contribution from the Western Mediterranean Oscillation. This near-linearity implies a predictable isotopic response to shifts in circulation regime that is comparatively insensitive to month-to-month variability in local precipitation totals. In the context of ongoing climate change, projections suggesting increased persistence or amplitude of positive NAO phases under anthropogenic forcing (López-Moreno et al. 2011; Smith et al. 2025) would, under the observed relationships, imply a tendency toward lower wet-season $\delta^{18}O$ in comparable SE Iberian recharge settings. Such changes would most plausibly reflect shifts in synoptic-scale organization, altering moisture pathways and the integrated condensation history, rather than being driven primarily by variability in local precipitation totals, reinforcing wet-season $\delta^{18}O$ as a sensitive tracer of circulation-state changes.

By contrast, the dry-season isotopic signal is structured by a different sensitivity. Here, precipitation amount overwhelmingly controls $\delta^{18}O$ variability, and the strongly non-linear response identified through SHAP diagnostics indicates regime behaviour: enriched isotopic values under low-precipitation conditions lead to rapid depletion as monthly rainfall increases, followed by saturation at higher amounts. This curvature is consistent with an amount-effect response characteristic of convective precipitation regimes. Under projected Mediterranean climate conditions marked by increased precipitation intermittency and a growing contribution from extreme events (Giorgi 2006; Pfahl et al. 2017), such non-linear behaviour implies that changes in dry-season rainfall structure may be preferentially amplified in isotopic records, even where seasonal precipitation totals remain comparatively stable.

These quantified seasonal relationships have also direct implications for paleoclimate significance of isotope-based archives from southeastern Iberia that can be extended to the western Mediterranean region. Speleothem and lacustrine isotopic records from the region document pronounced hydroclimatic variability throughout the Holocene, commonly interpreted in terms of shifts in atmospheric circulation and precipitation regime (Martín-Puertas et al., 2008; Sánchez-López et al., 2016; Gázquez et al., 2020; Cisneros et al., 2021; Gázquez et al., 2025). The seasonal separation identified here between circulation-dominated wet-season signals and amount-dominated dry-season signals provides a mechanistic framework for refining these interpretations. Archives preferentially derived from wet-season recharge, such as many Mediterranean speleothems, are therefore expected to preserve a stronger imprint of large-scale circulation variability, potentially reflecting past changes in the NAO and, at regional scale, the WeMO.

In contrast, systems integrating a larger contribution from dry-season conditions are more likely to encode variations in precipitation intensity and hydroclimatic extremes through amount-effect isotopic responses (Gázquez et al., 2025). Under this framework, coherent isotopic shifts in continental archives need not imply uniform hydrological changes but may instead reflect changes in the dominant season and atmospheric mechanism contributing to recharge, thereby improving interpretation of $\delta^{18}O$ variability under both present-day and late-Holocene climate conditions.

Another relevant implication of our results is that, within the observed NAO range, wet season $\delta^{18}O$ departs from the network mean by up to ±1.5‰ between strongly negative and strongly positive NAO conditions. Specifically, $\delta^{18}O$ in rainwater tends to be higher under negative NAO phases (NAOi ≤ -1) and lower under positive NAO phases (NAOi $\geq +1$), providing quantitative bounds on rainfall isotope variability that can be used to reduce uncertainty in isotope-enabled modelling and proxy-based reconstructions for SE Iberian recharge settings (Toney et al., 2020; Gázquez et al., 2020, 2025).

https://doi.org/10.5194/egusphere-2026-2058
Preprint. Discussion started: 12 May 2026
© Author(s) 2026. CC BY 4.0 License.

5 Conclusions

This study analyses the influence of atmospheric synoptic patterns (NAO and WeMO) on the isotopic composition of rainfall in southeastern Iberia, by integrating machine learning techniques and isotopic observational data from the Sierra de Segura (SE Spain). The main results derived from this work are the following:

1. The Western Mediterranean Oscillation index was extended beyond the temporal coverage of its original observational constraints by exploiting the shared regional pressure signal across multiple northern Italian stations. The proposed framework reproduces the published WeMOi with high fidelity at monthly resolution and largely preserves its dynamical structure, sign and amplitude without redefining its formulation or reprocessing historical datasets. The resulting hybrid series retains the previous published WeMOi unchanged up to 2020 and applies the reconstruction only beyond the observational endpoint, ensuring continuity with previous WeMO-based climatological studies while enabling analyses of recent hydroclimatic variability. Beyond this specific case, this strategy demonstrates how data-driven methods can preserve the operational relevance of circulation indices despite incomplete or evolving observational networks.
2. The Sierra de Segura precipitation-isotope network shows a high degree of internal coherence, with $\delta^{18}O$ capturing the dominant structure of the bulk isotopic system and yielding the most stable relationships with atmospheric predictors at monthly resolution. By contrast, ^{17}O-excess and d-excess display weaker and more heterogeneous coupling to large-scale drivers, consistent with additional sensitivity to kinetic and source–boundary-layer processes that are incompletely represented by monthly indices and precipitation totals; wet-season predictability is particularly low for ^{17}O-excess (Monte-Carlo $R^2 \approx 0.20$).
3. Across seasons, $\delta^{18}O$ exhibits a clear reorganization of controls: wet-season variability is primarily circulation-driven, dominated by the NAO with a secondary WeMO modulation, whereas dry-season variability is organized by precipitation amount through a strongly non-linear, amount-effect response characteristic of convective regimes. The convergence of correlation patterns, PCA structure and explainable machine-learning diagnostics confirms that the isotope signal is controlled not only by different dominant predictors across seasons, but also by distinct response shapes that depend on precipitation regime. These inferences are strongest for the wet-season regime, whereas dry-season transport diagnostics and excess-metric attribution remain more uncertain due to fewer events and stronger mesoscale variability.
4. The quantification of how circulation and precipitation regimes are encoded in precipitation $\delta^{18}O$ provides a process-based framework for interpreting isotopic variability across different timescales in the western Mediterranean and for linking precipitation signals to the meteoric recharge recorded by continental paleoclimate archives. The near-linear sensitivity of wet-season $\delta^{18}O$ to large-scale circulation implies that changes in the frequency or persistence of circulation modes, such as the NAO, can translate into systematic shifts in the isotopic baseline even in the absence of major changes in precipitation totals. In contrast, the strongly non-linear dry-season response to precipitation amount highlights the sensitivity of isotopic records to changes in rainfall structure, intermittency and hydroclimatic extremes.
5. Overall, these findings refine the interpretation of isotope signals in both modern observations and paleoclimate archives, by enabling circulation-driven variability to be distinguished from precipitation-regime effects associated with convective processes across the Holocene and into the ongoing anthropogenic climate change. Identifying the seasonal and functional controls on isotopic variability provides a robust basis for a more accurate interpretation of Mediterranean paleoclimate records, reconciling apparent inconsistencies among them, particularly where wet-season circulation and dry-season hydroclimatic extremes exert competing influences. This approach is readily transferable to other climatically complex regions influenced by multiple modes of atmospheric variability.

Code availability

The code and processed data supporting this study are archived in Zenodo at https://zenodo.org/records/19075045. The repository includes the scripts used for the analyses and figure generation, together with the processed datasets required to reproduce the results.

Supplement link

The link to the supplement will be included by Copernicus, if applicable.

Author contributions

AS and FG: Conceptualization. AS: Data curation, Formal analysis, Investigation, Methodology, Software, Visualization, Writing (original draft preparation). ALMG: Investigation (field campaign design, execution and sample collection). ALMG and FG: Investigation (isotopic analysis). FG, JMC and MM: Funding acquisition, Supervision. AGR: Resources, Investigation. FMM: Resources, Investigation. RJE: Resources, Investigation. All authors contributed to Writing (review and editing) and approved the final version of the manuscript.

Competing interests

The authors declare no competing interests.

Disclaimer

Copernicus Publications remains neutral with regard to jurisdictional claims made in the text, published maps, institutional affiliations, or any other geographical representation in this paper. While Copernicus Publications makes every effort to include appropriate place names, the final responsibility lies with the authors. Views expressed in the text are those of the authors and do not necessarily reflect the views of the publisher.

Acknowledgements

We gratefully acknowledge J.A. López-Bustins for generously sharing historical documentation and for providing key methodological clarifications on the original WeMO formulation, which greatly strengthened the conceptual basis and extension of the index presented in this study. We also thank the *Agencia Estatal de Meteorología* (AEMET) and the *Agenzia Regionale per la Prevenzione e Protezione Ambientale del Veneto* (ARPAV) for making available the meteorological data used in this work. In addition, we thank L. Calabrò for her help in identifying suitable stations in the Veneto region and for her guidance in tracing the relevant regional data sources.

Financial support

This study was funded by the GYPCLIMATE (PID2021-123980OA-I00), PALEONET (RED24-153734- T), CLIMGYP (CNS2025-165139), CALACLIMP (PID2021-122854OB-I00) of the Spanish Ministry of Science, Innovation and Universities. F.G acknowledges the Ramón y Cajal contract (RYC2020-029811-I) and the PPIT-UAL grant from the Andalusian Regional Government -FEDER2022-2026 (RyC-PPI2021-01). A.S. acknowledges the FPI predoctoral contract (PRE2022-101561) from the Spanish Ministry of Science and Innovation.

© Author(s) 2026. CC BY 4.0 License.

Review statement

The review statement will be added by Copernicus Publications listing the handling editor as well as all contributing referees according to their status anonymous or identified.

References

Bowen, G. J. Isoscapes: Spatial pattern in isotopic biogeochemistry. Annu. Rev. Earth Planet. Sci. 38, 161–187 (2010). https://doi.org/10.1146/annurev-earth-040809-152429

Bowen, G. J. & Wilkinson, B. Spatial distribution of δ¹⁸O in meteoric precipitation. Geology 30, 315–318 (2002). https://doi.org/10.1130/0091-7613(2002)030<0315:SDOOIM>2.0.CO;2

Chazarra-Bernabé, A., Mestre-Barceló, C., & Rodríguez-Ballesteros, R. (2018). Atlas climático ibérico. Temperatura y precipitación (1971–2000).

Agencia Estatal de Meteorología (AEMET), Ministerio para la Transición Ecológica, Madrid.

Chen, T. & Guestrin, C. XGBoost: A scalable tree boosting system. In Proc. 22nd ACM SIGKDD Int. Conf. on Knowledge Discovery and Data Mining 785–794 (ACM, 2016). https://doi.org/10.1145/2939672.2939785

Cisneros, M., Cacho, I., Moreno, A. et al. Hydroclimate variability during the last 2700 years based on stalagmite multi-proxy records in the central-western Mediterranean. Quat. Sci. Rev. 269, 107137 (2021). https://doi.org/10.1016/j.quascirev.2021.107137

Clark, I. D., & Fritz, P. (1997). Environmental Isotopes in Hydrogeology.CRC Press, Boca Raton.Dabrio, 1973. ISBN: 978-1-56670-249-2

Dansgaard, W. Stable isotopes in precipitation. Tellus 16, 436–468 (1964). https://doi.org/10.1111/j.2153-3490.1964.tb00181.x

De Luis, M., González-Hidalgo, J. C., Brunetti, M. & Longares, L. A. Precipitation concentration changes in Spain 1946–2005. Nat. Hazards Earth Syst. Sci. 11, 1259–1265 (2011). https://doi.org/10.5194/nhess-11-1259-2011

Díaz-Teijeiro, M. F., Araguás-Araguás, L. & Rozanski, K. Stable isotopes in precipitation over Spain: Spatial distribution and temporal variability. In Isotopic Composition of Precipitation in the Mediterranean Basin in Relation to Air Circulation Patterns and Climate (IAEA-TECDOC-1453), 173–190 (IAEA, Vienna, 2005).

Dorling, S. R., Davies, T. D. & Pierce, C. E. Cluster analysis: A technique for estimating the synoptic meteorological controls on air and precipitation chemistry—method and applications. Atmos. Environ. Part A 26, 2575–2581 (1992). https://doi.org/10.1016/0960-1686(92)90110-7

Fairchild, I. J. & Baker, A. Speleothem Science: From Process to Past Environments. Wiley-Blackwell (2012). ISBN: 978-1-4051-9620-8

Gat, J. R. Oxygen and hydrogen isotopes in the hydrologic cycle. Annu. Rev. Earth Planet. Sci. 24, 225–262 (1996). https://doi.org/10.1146/annurev.earth.24.1.225

Gázquez, F., Bauska, T. K., Comas-Bru, L., Ghaleb, B., Calaforra, J.-M. & Hodell, D. A. The potential of gypsum speleothems for paleoclimatology: Application to the Iberian Roman Humid Period. Sci. Rep. 10, 14705 (2020). https://doi.org/10.1038/s41598-020-71679-3

Gázquez, F., Voigt, C., Castillo, A. et al. Quantifying atmospheric humidity in the western Mediterranean during the Iron Age and the Roman Era. Geophys. Res. Lett. (2025). https://doi.org/10.1029/2025GL120424

Geurts, P., Ernst, D. & Wehenkel, L. Extremely randomized trees. Mach. Learn. 63, 3–42 (2006). https://doi.org/10.1007/s10994-006-6226-1

Giménez Reyes, R., Bartolomé, M., Gázquez, F., Iglesias, M. & Moreno, A. Underlying climate controls in triple oxygen (^{16}O, ^{17}O, ^{18}O) and hydrogen (^{1}H, ^{2}H) isotopes composition of rainfall (Central Pyrenees). Front. Earth Sci. 9, 633698 (2021). https://doi.org/10.3389/feart.2021.633698

Giorgi, F. Climate change hot-spots. Geophys. Res. Lett. 33, L08707 (2006). https://doi.org/10.1029/2006GL025734

González-Hidalgo, J. C., Brunetti, M., & De Luis, M. (2011). A new tool for monthly precipitation analysis in Spain: MOPREDAS database (monthly precipitation trends December 1945–November 2005). International Journal of Climatology, 31(5), 715–731. https://doi.org/10.1002/joc.2115

Hatvani, I. G., Szatmári, G., Kern, Z., Erdélyi, D., Vreča, P., Kanduč, T., Czuppon, G., Lojen, S., & Kohán, B. (2020). Geostatistical evaluation of the design of the precipitation stable isotope monitoring network for Slovenia and Hungary. Environment International, 145, 106263. https://doi.org/10.1016/j.envint.2020.106263

Hernández, A., Sánchez-López, G., Pla-Rabes, S., Comas-Bru, L., Parnell, A., Cahill, N., Geyer, A., Trigo, R. M., & Giralt, S. (2020). A 2,000-year Bayesian NAO reconstruction from the Iberian Peninsula. Scientific Reports, 10, Article 14961. https://doi.org/10.1038/s41598-020-71372-5

Hurrell, J. W. Decadal trends in the North Atlantic Oscillation: Regional temperatures and precipitation. Science 269, 676–679 (1995). https://doi.org/10.1126/science.269.5224.676

Leng, M. J., & Marshall, J. D. (2004). Palaeoclimate interpretation of stable isotope data from lake sediment archives. Quaternary Science Reviews, 23(7–8), 811–831. https://doi.org/10.1016/j.quascirev.2003.06.012

López-Bustins, J. A., Martin-Vide, J., & Sánchez-Lorenzo, A. (2008). Iberia winter rainfall trends based upon changes in teleconnection and circulation patterns. Global and Planetary Change, 63(2–3), 171–176. https://doi.org/10.1016/j.glopacha.2007.09.002

López-Bustins, J. A., Arbiol-Roca, L., Martin-Vide, J., Barrera-Escoda, A., & Prohom, M. (2020). Intra-annual variability of the Western Mediterranean Oscillation (WeMO) and occurrence of extreme torrential precipitation in Catalonia (NE Iberia). Natural Hazards and Earth System Sciences, 20, 2483–2501. https://doi.org/10.5194/nhess-20-2483-2020

Lopez-Bustins, J. A., & Lemus-Canovas, M. (2020). The influence of the Western Mediterranean Oscillation upon the spatio-temporal variability of precipitation over Catalonia (northeastern Iberian Peninsula). Atmospheric Research, 234, 104819. https://doi.org/10.1016/j.atmosres.2019.104819

López-Moreno, J. I., Vicente-Serrano, S. M., Morán-Tejeda, E., Lorenzo-Lacruz, J., Kenawy, A. & Beniston, M. Effects of the North Atlantic Oscillation (NAO) on combined temperature and precipitation winter modes in the Mediterranean mountains: Observed relationships and projections for the 21st century. Glob. Planet. Change 77, 62–76 (2011). https://doi.org/10.1016/j.gloplacha.2011.03.003

Luz, B. & Barkan, E. Variations of ^{17}O/^{16}O and ^{18}O/^{16}O in meteoric waters. Geochim. Cosmochim. Acta 74, 6276–6286 (2010). https://doi.org/10.1016/j.gca.2010.08.016

Martín-Puertas, C., Valero-Garcés, B. L., Mata, M. P. et al. Arid and humid phases in southern Spain during the last 4000 years: The Zoñar Lake record, Córdoba. Holocene 18, 907–921 (2008). https://doi.org/10.1177/0959683608093533

Martín-Vide, J. & López-Bustins, J.-A. The Western Mediterranean Oscillation and rainfall in the Iberian Peninsula. Int. J. Climatol. 26, 1455–1475 (2006). https://doi.org/10.1002/joc.1388

J. Martín-Vide, A. Sanchez-Lorenzo, J.A. Lopez-Bustins, M.J. Cordobilla, A. Garcia-Manuel, J.M. Raso. Torrential rainfall in northeast of the Iberian Peninsula: synoptic patterns and WeMO influence. Adv. Sci. Res., 2 (2008), pp. 99-105. https://doi.org/10.5194/asr-2-99-2008

McDermott, F. Palaeo-climate reconstruction from stable isotope variations in speleothems: a review. Quat. Sci. Rev. 23, 901–918 (2004). https://doi.org/10.1016/j.quascirev.2003.06.021

Morellón, M., Pérez-Sanz, A., Corella, J. P., Büntgen, U., Catalán, J., González-Sampériz, P., González-Trueba, J. J., López-Sáez, J. A., Moreno, A., Pla-Rabes, S., Saz-Sánchez, M. Á., Scussolini, P., Serrano, E., Steinhilber, F., Stefanova, V., Vegas-

Vilarrúbia, T., and Valero-Garcés, B.: A multi-proxy perspective on millennium-long climate variability in the Southern Pyrenees, Clim. Past, 8, 683–700, https://doi.org/10.5194/cp-8-683-2012 , 2012.

Moreno, A., Pérez, A., Frigola, J., Nieto-Moreno, V., Rodrigo-Gámiz, M., Martrat, B., González-Sampériz, P., Morellón, M., Martín-Puertas, C., Corella, J. P., Belmonte, Á., Sancho, C., Cacho, I., Herrera, G., Canals, M., Grimalt, J. O., Jiménez-Espejo, F., Martínez-Ruiz, F., Vegas-Vilarrúbia, T., & Valero-Garcés, B. L. (2012). The Medieval Climate Anomaly in the Iberian Peninsula reconstructed from marine and lake records. Quaternary Science Reviews, 43, 16–32. https://doi.org/10.1016/j.quascirev.2012.04.007

Moreno, A., Iglesias, M., Azorin-Molina, C., Pérez-Mejías, C., Bartolomé, M., Sancho, C., Stoll, H., Cacho, I., Frigola, J., Osácar, C., Muñoz, A., Delgado-Huertas, A., Bladé, I. & Vimeux, F. Measurement report: Spatial variability of northern Iberian rainfall stable isotope values – investigating atmospheric controls on daily and monthly timescales. Atmos. Chem. Phys. 21, 10159–10177 (2021). https://doi.org/10.5194/acp-21-10159-2021

Natali, S., Doveri, M., Giannecchini, R., Baneschi, I. & Zanchetta, G. Is the deuterium excess in precipitation a reliable tracer of moisture sources and water resources fate in the western Mediterranean? New insights from Apuan Alps (Italy). J. Hydrol. 612, 128497 (2022). https://doi.org/10.1016/j.jhydrol.2022.128497

Pereira, S. C., Carvalho, D., & Rocha, A. (2021). Temperature and precipitation extremes over the Iberian Peninsula under climate change scenarios: a review. Climate, 9(9), 139. https://doi.org/10.3390/cli9090139

Pfahl, S. & Sodemann, H. What controls deuterium excess in global precipitation? Clim. Past 10, 771–781 (2014). https://doi.org/10.5194/cp-10-771-2014

Pfahl, S. & Sodemann, H. What controls deuterium excess in global precipitation? Clim. Past 10, 771–781 (2014). https://doi.org/10.5194/cp-10-771-2014

Quesada, B.; Vautard, R.; Yiou, P.; Hirschi, M.; Seneviratne, S. Asymmetric European summer heat predictability from wet and dry southern winters and springs. Nat. Clim. Chang. 2012, 2, 736–741. https://doi.org/10.1038/nclimate1536

Risi, C., Bony, S. & Vimeux, F. Influence of convective processes on the isotopic composition ($\delta^{18}O$ and δD) of precipitation and water vapour in the tropics: 2. Physical interpretation of the amount effect. J. Geophys. Res. Atmos. 113, D19306 (2008). https://doi.org/10.1029/2008JD009943

Rozanski, K., Araguás-Araguás, L. & Gonfiantini, R. Isotopic patterns in modern global precipitation. In Climate Change in Continental Isotopic Records (eds Swart, P. K., Lohmann, K. C., McKenzie, J. & Savin, S.) Geophys. Monogr. Ser. 78, 1–36 (AGU, 1993). https://doi.org/10.1029/GM078p0001

Sánchez-López, G., Hernández, A., Pla-Rabes, S. et al. Climate reconstruction for the last two millennia in central Iberia: The role of East Atlantic (EA), North Atlantic Oscillation (NAO) and their interplay over the Iberian Peninsula. Quat. Sci. Rev. 149, 135–150 (2016). https://doi.org/10.1016/j.quascirev.2016.07.021

Schoenemann, S. W., Schauer, A. J. & Steig, E. J. Measurement of SLAP2 and GISP $\delta^{17}O$ and proposed VSMOW–SLAP normalization for $\delta^{17}O$ and ^{17}O-excess. Rapid Commun. Mass Spectrom. 27, 582–590 (2013). https://doi.org/10.1002/rcm.6486

Serrano-Notivoli, R., Beguería, S., de Luis, M., González-Hidalgo, J. C. & Vicente-Serrano, S. M. Trends and variability of monthly precipitation in the Iberian Peninsula (1950–2012). Int. J. Climatol. 38, 549–563 (2018). https://doi.org/10.1002/joc.5387

Smith, D. M., Dunstone, N. J., Eade, R. et al. Mitigation needed to avoid unprecedented multi-decadal North Atlantic Oscillation magnitude. Nat. Clim. Change 15, 403–410 (2025). https://doi.org/10.1038/s41558-025-02277-2

Steig, E. J., Gkinis, V., Schauer, A. J., Schoenemann, S. W., Samek, K., Hoffnagle, J., Dennis, K. J. & Tan, S. Calibrated high-precision ^{17}O-excess measurements using cavity ring-down spectroscopy with laser-current-tuned cavity offset. Atmos. Meas. Tech. 7, 2421–2435 (2014). https://doi.org/10.5194/amt-7-2421-2014

© Author(s) 2026. CC BY 4.0 License.

Stein, A. F., Draxler, R. R., Rolph, G. D., Stunder, B. J. B., Cohen, M. D. & Ngan, F. NOAA's HYSPLIT atmospheric transport and dispersion modeling system. Bull. Am. Meteorol. Soc. 96, 2059–2077 (2015). https://doi.org/10.1175/BAMS-D-14-00110.1

Toney, J. L., García-Alix, A., Jiménez-Moreno, G., Anderson, R. S., Moossen, H. & Seki, O. New insights into Holocene hydrology and temperature from lipid biomarkers in western Mediterranean alpine wetlands. Quat. Sci. Rev. 240, 106395 (2020). https://doi.org/10.1016/j.quascirev.2020.106395

Trigo, R.M., Pozo-Vázquez, D., Osborn, T.J., Castro-Díez, Y., Gámiz-Fortis, S. and Esteban-Parra, M.J. (2004), North Atlantic oscillation influence on precipitation, river flow and water resources in the Iberian Peninsula. Int. J. Climatol., 24: 925-944. https://doi.org/10.1002/joc.1048

Trigo, R. M., Osborn, T. J. & Corte-Real, J. M. The North Atlantic Oscillation influence on Europe: Climate impacts and associated physical mechanisms. Clim. Res. 20, 9–17 (2002). https://doi.org/10.3354/cr020009

Uechi, Y. & Uemura, R. Atmospheric processes controlling spatial and seasonal variation in ^{17}O-excess of precipitation over Japan. Earth Planet. Sci. Lett. 513, 56–65 (2019). https://doi.org/10.1016/j.epsl.2019.02.012